

# Linear Algebraic Calculation of Green's function for Large-Scale Electronic Structure Theory

R. Takayama<sup>1,2</sup>, T. Hoshi<sup>2,3</sup>, T. Sogabe<sup>2</sup>, S.-L. Zhang<sup>2</sup>, and T. Fujiiwara<sup>2,3</sup>

<sup>1</sup> Research and Development for Applying Advanced Computational Science and Technology (ACT-JST), Japan Science and Technology Agency, 4-1-8 Honcho, Kawaguchi-shi, Saitama 332-0012, Japan

<sup>2</sup> Department of Applied Physics, University of Tokyo, 7-3-1 Hongo, Bunkyo-ku, Tokyo 113-8656, Japan

<sup>3</sup> Core Research for Evolutional Science and Technology (CREST-JST), Japan Science and Technology Agency  
(Dated: March 19, 2019)

A linear algebraic method named the shifted conjugate-orthogonal-conjugate-gradient method is introduced for large-scale electronic structure calculation and molecular dynamics simulation. Present method reduces the calculation of Green's functions to the iterative procedure of independent linear equations and the proposed algorithm needs the calculation of only a single reference energy point rather than many energy points. The method is robust against the round-off error and the calculation can reach the machine accuracy. Since the residual of the iterative procedure provides rigorous estimation of error, the number of iteration steps for convergence can be controlled, dynamically and independently for each element of the Green's function, during the molecular dynamics simulation. The method is applied to both semiconductor and metal.

PACS numbers: 71.15.m, 71.15.Nc, 71.15.Pd

## I. INTRODUCTION

Large-scale atomistic simulation with quantum mechanical freedom of electrons requires manipulation of a large Hamiltonian matrix. In order to calculate physical quantities of a system, we should obtain either eigenstates or the density matrix of the system. The calculation of eigenstates is usually reduced to matrix diagonalization procedure and this procedure results in severe computational cost for a large-scale system.

Any physical quantity  $X$  can be evaluated by means of the density matrix as

$$X = \int d\mathbf{r} d\mathbf{r}' \langle \mathbf{r}; \mathbf{r}' | X | \mathbf{r}', \mathbf{r} \rangle. \quad (1)$$

Even though the density matrix is of long-range, only the short-range behavior of the density matrix is necessary in case that  $X$  is a short-range operator. The energy and forces acting on an individual atom are really this case, and the locality of the Hamiltonian has this advantage in large-scale calculation. Therefore, the essential methodology for large-scale electronic structure calculation is how to obtain the density matrix without calculating eigenstates. [1, 2, 3, 4, 5, 6, 7, 8, 9, 10, 11, 12, 13]

We have developed a set of methods for large-scale atomistic simulation without calculating eigenstates in fully quantum mechanical description of electron systems. [6, 7, 8, 9, 10, 11] Among them, the subspace diagonalization method based on the Krylov subspace (SD-KS method) was introduced, where the original Hamiltonian matrix  $H$  is reduced to a small size easy-tractable one and

its diagonalization leads to approximation of the density matrix of the original system. [11] The SD-KS method is suitable to the quantum mechanical molecular dynamics simulation but is problematic in robustness if one would require a very fine structure of spectrum. This is because the SD-KS method is affected sensitively by round-off error.

The present strategy to obtain the Green's function and the density matrix is to introduce first a procedure to solve linear equations with a given orbital  $j_i$ :

$$(z - H) \mathbf{x}_{ji} = \mathbf{j}_i. \quad (2)$$

The method should be iterative and not require inversion of matrices. Once the linear equation is solved, one can obtain any element of the Green's function as

$$G_{ij}(z) = h_{ij}(z - H)^{-1} \mathbf{j}_i = h_{ij} \mathbf{x}_{ji}. \quad (3)$$

The complex energy  $z = \epsilon + i\Gamma$  is introduced for numerical energy integration to obtain the one-body density matrix;

$$_{ij} = \frac{1}{\Gamma} \int_{\epsilon}^{z-1} \text{Im} G_{ij}(z) f \left( \frac{\epsilon}{k_B T} \right) d\epsilon; \quad (4)$$

where  $f(x)$  is the Fermi distribution function. The chemical potential is determined so that the sum of the diagonal elements of the density matrix equals the total number of electrons.

The aim of the present paper is to introduce the shifted conjugate-orthogonal-conjugate-gradient (CO-CG) method with shifted linear systems [14, 15] to obtain the density matrix in large-scale electronic structure calculation. The first important point of this novel method is the robustness against round-off error and the calculation can reach the machine accuracy. The second important one is to know the numerical accuracy

Present address: Canon Inc., Analysis technology center, 5-1 Morinosato-Wakamiya, Atsugi-shi, Kanagawa 243-0193, Japan

or to monitor a residual error during the simulation which is essential advantage in large-scale calculation. The third important one is that the present method can be used both for metallic and insulating systems. In Sec. II, the Krylov subspace will be first explained and, then, the shifted COCG method will be introduced. In Sec. III, the residual norm will be introduced to estimate the accuracy of the Green's function. Behavior of the RN with iteration steps is demonstrated and the number of operations in actual calculation is discussed. Section IV will be devoted to application of the present method to atomic scale reconstruction and electronic structure of semiconductor surface (silicon) and the bulk electronic structure of metal (copper). In Sec. V, the summary will be given. The details of algorithm of the shifted COCG method will be explained in Appendix A. In Appendix B, the subspace-diagonalization method (the SD-KS method) will be explained and reanalyzed.

## II. SHIFTED CONJUGATE ORTHOGONAL CG METHOD

### A. Krylov subspace

In order to solve eq. (2), we will adopt an iterative procedure for linear equations. In the present case, though the Hamiltonian  $H$  is real symmetric,  $(z - H)$  is complex symmetric but not Hermitian because of a complex energy  $z = ! + i$ . Then the conjugate orthogonal conjugate gradient method (COCG method) can be used. [15]

For an arbitrary operator  $A$ , a set of states (vectors)  $fA^n jji$  is named the Krylov subspace (KS), and represented as

$$K(A; jji) = \text{span } jji; A jji; A^2 jji; \dots; A^{-1} jji; \quad (5)$$

where  $n$  is the dimension of the KS. The iterative methods based on the KS are generally called the Krylov subspace method. [14, 16] The solution vector of eq. (2),  $jki = (z - H)^{-1} jji$ , is constructed within the KS  $K(z - H; jji)$ .

### B. Shifted COCG method

The COCG method can be used to solve the large scale linear equations without inversion of large matrices. Even so, matrix-vector multiplication at every energy point is still very heavy time-consuming procedure and the reduction of computational cost is crucial. The shifted COCG method is an extension of the COCG method by means of the algorithm of shifted linear systems. The KS for the shifted system is identical to that of the reference system when the initial residual vectors for both systems are the same. This fact can reduce the computational cost drastically.

We follow Refs. [17, 18] to formulate the shifted COCG method and consider two systems

$$(z_{\text{ref}} - H) jk^{(j)} (z_{\text{ref}}) i = jji; \quad (6)$$

$$(z_{\text{ref}} + \kappa H) jk^{(j)} (z_{\text{ref}} + \kappa H) i = jji; \quad (7)$$

corresponding to the energies  $!_{\text{ref}}$  ( $z_{\text{ref}} = !_{\text{ref}} + i$ ) and  $!_{\text{ref}} + \kappa$ . The systems (6) and (7) will be termed the reference and the shifted systems, respectively. The shifted parameter  $\kappa$  is a variable and  $!_{\text{ref}} + \kappa$  covers the whole energy range interested in.

The central idea of the shifted linear system is based on the following three facts; (i) an approximate solution from the  $n$ -th step of the iterative algorithm can be expressed in the KS  $K_n(z_{\text{ref}} - H; jji)$ , (ii) a shifted matrix generates the same Krylov subspace with respect to any fixed vector  $jji$ , and (iii) the above facts (i) and (ii) lead to a collinear relation between the residual vectors generated in the two systems and this provides a key information of correspondence between the two systems.

Equation (6) is solved iteratively for which the  $n$ -th iterated solution  $jk^{(j)}_n i$  is contained in  $jk^{(j)}_0 i + K_n(z_{\text{ref}} - H); jk^{(j)}_0 i$ , with  $jk^{(j)}_0 i = jji$  ( $z_{\text{ref}} - H) jk^{(j)}_0 i$  being an initial residual belonging to the initial guess  $jk^{(j)}_0 i$ . Each iterative step requires, at least, one matrix-vector multiplication with  $(z_{\text{ref}} - H)$  in order to update the basis of  $K_n$  to that of  $K_{n+1}$ . Similar relation can be held for the solution vector  $jk^{(j)}_n i$  and the residual vector  $jk^{(j)}_n i$  of the shifted system, eq. (7). Now assume that we take initial guesses  $jk^{(j)}_0 i = 0$  and  $jk^{(j)}_0 i = 0$  for the reference and the shifted systems, respectively. Then the initial residual satisfies  $jk^{(j)}_0 i = jk^{(j)}_0 i = jji$ . Since shifted matrices generate the same Krylov subspace with respect to the fixed vector  $jji$ ;

$$K_n(z_{\text{ref}} - H; jji) = K_n(z_{\text{ref}} + \kappa H; jji); \quad (8)$$

then  $jk^{(j)}_n i$  and  $jk^{(j)}_n i$  for the reference and the shifted systems are generated from the same Krylov subspace. Consequently, the time consuming matrix-vector multiplications to update the KS are needed only for the reference system. The detail description of the shifted COCG method are given in Appendix A 1 and the number of algebraic operations will be discussed in Sec. III C.

## III. RESIDUAL NORMS AND NUMBER OF OPERATIONS IN THE SHIFTED COCG METHOD

### A. Definition of residual norm

In order to estimate the convergence of the calculation, we define the residual vector at the  $n$ -th iteration, as

$$jk^{(j)}_n i = jji - (z_{\text{ref}} + \kappa H) jk^{(j)}_n i; \quad (9)$$

The residual vector becomes zero when  $n = M$ , where the size of the original Hamiltonian matrix  $H$  is  $M \times M$ .

The residual vector in the shifted system is related to that in the reference system with the shift coefficient  $\tau_n$  (see eq. (A 10)) as

$$\mathbf{j}_{\mathbf{n}}^{(j)} \mathbf{i} = \mathbf{j}_{\mathbf{n}}^{(j)} \mathbf{i} \frac{1}{\tau_n}; \quad (10)$$

Owing to this collinear relation, the choice of the reference energy does not affect the calculated results of the density matrix or the residual vector.

Because we need only the elements of the density matrix of near-sited orbital pairs in eq. (1), we define a residual norm (RN) for the reference and the shifted system  $s$ , respectively, as

$$\mathbf{j}_{\mathbf{n}}^{(j)} \mathbf{j}^2 = \sum_{i,j} M_{int} \mathbf{j}_{ii} \mathbf{j}_{nn}^{(j)} \mathbf{j}_{jj}^2; \quad (11)$$

$$\mathbf{j}_{\mathbf{n}}^{(j)} \mathbf{j}^2 = \sum_{i,j} M_{int} \mathbf{j}_{ii} \mathbf{j}_{nn}^{(j)} \mathbf{j}_{jj}^2; \quad (12)$$

where, for a fixed  $jji$ , the number of interacting orbitals  $jji$  is  $M_{int}$  ranging from 1 to about 100. The convergence is necessary only for elements of the density matrix of near-sited orbital pairs needed in calculation of required physical properties but not for far-distanted ones not used in calculation.

It is necessary to integrate the Green's function over  $N_{ene}$  energy points to obtain the density matrix and we need to know the convergence behavior of the RN over the whole band region during calculation. Then we average this quantity for a fixed  $j$  over the energy range between  $E_{max}$  and  $E_{min}$  or the shift parameter  $\tau$ , and the resultant quantity is named the energy-averaged residual norm (a-RN);

$$R_n^{(j)} = \frac{1}{E_{max} - E_{min}} \int_{E_{min}}^{E_{max}} dE \mathbf{j}_{\mathbf{n}}^{(j)} \mathbf{j}^2; \quad (13)$$

The a-RN can be monitored for each atom  $i$  site or orbital  $jji$  during simulation, then the optimal number of iterations can be determined locally for individual orbital. From eqs. (10) and (13), the a-RN  $R_n^{(j)}$  can be expressed by using the RN of the reference system  $\mathbf{j}_{\mathbf{n}}^{(j)} \mathbf{j}^2$  in the following way:

$$R_n^{(j)} = \frac{1}{E_{max} - E_{min}} \int_{E_{min}}^{E_{max}} dE \mathbf{j}_{\mathbf{n}}^{(j)} \mathbf{j}^2; \quad (14)$$

$$R_n^{(j)} = \frac{1}{E_{max} - E_{min}} \int_{E_{min}}^{E_{max}} \frac{1}{\tau_n^2} d\tau_n: \quad (15)$$

## B. Behavior of residual norm

As an example, we calculated the electronic structure in a bulk Si system of 512 atoms with the transferable tight-binding Hamiltonian, [19] which is a  $M \times M$  matrix of  $M = 4 \times 512 = 2048$ . The energy spectrum was

obtained at  $N_{ene} = 1000$  energy points in the band region and consists of a set of spikes with a small width  $\Delta E = 0.002$  eV. See the imaginary part of the Green's function in Fig. 6(a) in Appendix A 2.

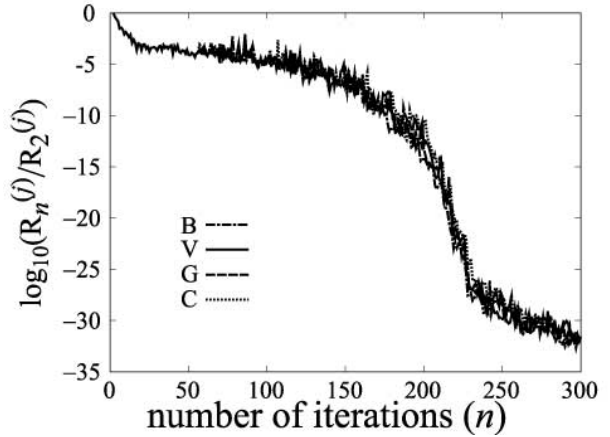


FIG. 1: Energy-averaged residual norm a-RN for a system of Si512 atoms. Four lines for different reference energies B, V, G and C shown in Fig. 6 follow the same curve.

The choice of the reference energy is arbitrary and the present scheme of the algorithm is quite robust for the numerical calculation. Figure 1 shows the iteration dependence of the a-RN for four different reference energy points B, V, G and C, and all cases actually follow the same curve till the machine accuracy. Even when we choose the reference energy at the bottom of the band region (B), the calculation can be achieved though both the RN  $\mathbf{j}_{\mathbf{n}}^{(j)} \mathbf{j}^2$  and the shift coefficient  $\tau_n$  go to the order of  $10^{-250}$  when the number of iteration steps reaches 300. See details in Appendix A 2. The behavior of the a-RN is shown also in Fig. 2 for the system of Si512 atoms and the RN reaches a steady stage when the number of iteration steps is about 50. After that, the a-RN starts decrease again to the machine accuracy as in Fig. 1. The iteration steps of  $n = 30 - 50$  is enough for actual calculation.

The convergence behavior was studied also in metals. The system is a bulk fcc Cu of 1568 atoms. We adopt the second-order Hamiltonian  $H^{(2)}$  of the tight-binding LMTO method. [20] This Hamiltonian is of very simple form but the resultant spectrum is reliable in the energy region of 10 eV around the Fermi energy. See the partial DOS in Fig. 4. The orbital dependence of the a-RN ( $s$  and  $t_{2g}$  states) is shown in Fig. 2. The calculation starts from local muffin-tin orbital basis  $\mathbf{j}_{si}$ ,  $\mathbf{j}_{pi}$ ,  $\mathbf{j}_{d(t_{2g})i}$ , and  $\mathbf{j}_{l(e_g)i}$ , respectively. There is no essential difference between behavior of spatial extent of basis orbitals in semiconductors and metals or in different symmetry of orbitals, since any system can be described by the short-ranged tight-binding Hamiltonian as here. In fact, though each a-RN in Fig. 2 decays differently at small number of iteration steps, their behaviour for larger number of iteration steps becomes similar in

magnitude. A accuracy estimation by the a-RN is great advantage from practical viewpoint, comparing to other methods with matrix-vector operations, e.g. the Chebyshev polynomial representations [12, 13] and the recursion method. [2]

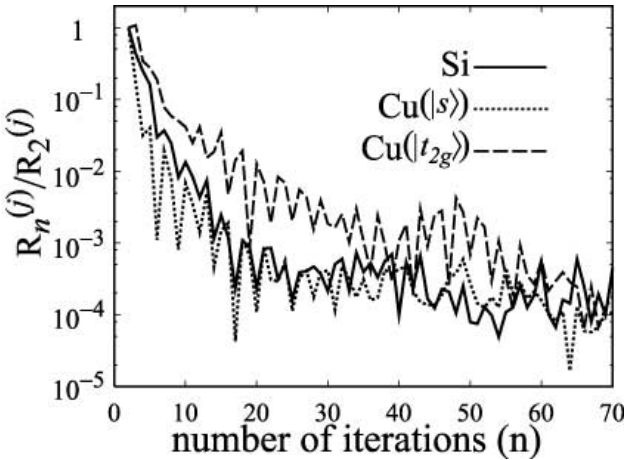


FIG. 2: Iteration dependence of the a-RN in a system of Si 512 atoms and those of local  $s$  and  $t_{2g}$  states in a system of Cu 1568 atoms.

### C. Number of matrix-vector operations

The present method allows us large reduction of time in the practical molecular dynamics simulation. The estimation of numbers of operations for one iteration is summarized in Table I. In the COCG method, the matrix-vector product is the main contribution. In the

M method	Inner P roduct	Scalar-Vector P roduct	M atrix-Vector P roduct
COCG	$3M N_{\text{ene}}$	$3M N_{\text{ene}}$	$M M_{\text{int}} N_{\text{ene}}$
shifted COCG (total)	$3M$	$3M N_{\text{ene}}$	$M M_{\text{int}}$
shifted COCG (present)	$3M$	$3M_{\text{int}} (N_{\text{ene}} - 1) + 3M$	$M M_{\text{int}}$

TABLE I: Summary of numbers of operations for one iteration step. Operations of "Inner P roduct" (the second column) are in eqs. (A 4) and (A 5), those of "Scalar-Vector P roduct" (the third column) in eqs. (A 1), (A 2), (A 3) and (A 7), (A 8), (A 10) and those of "M atrix-Vector P roduct" (the fourth column) in  $A p_n$  of eq. (A 4). Here, in the first column and the third row, a term "total" means the procedure of calculating "all" elements of the density matrix and the RN (not only elements within the interaction range as stated in the text and eqs. (11) and (12)). A term "present" means just the present shifted COCG method.  $M$  : the dimension of the original Hamiltonian matrix,  $M_{\text{int}}$  : the number of orbitals within interaction range.

shifted COCG method, the contribution from the matrix-vector multiplication is reduced to  $1=N_{\text{ene}}$  and the operation of the scalar-vector products ( $\times$ ) becomes the most time-consuming. In the present formulation of the shifted linear system, the updating cost of the vectors  $x_n$ ,  $p_n$ , and  $r_n$  are common to those of reference systems and, therefore, the algorithm requires operations as many times as the size of  $M \times M$  matrices. The reduction of the computation time is restricted within a part of updating these vectors. In actual calculation, we use the short-ranged tight-binding Hamiltonian and, therefore, we need update only orbitals within interaction range used in the RN. The shifted COCG method combined with the locality of the Hamiltonian, with monitoring the RN, reduces computation time drastically as listed in Table I.

We note here that the computational program of the present Green's function method can be parallelized easily due to its nature of independency with respect to a basis  $jj$ .

## IV. APPLICATIONS TO ELECTRONIC STRUCTURE CALCULATION

The shifted COCG method with the a-RN was applied to two cases of electronic structure calculation; a semiconductor Si slab of 1024 atoms with the asymmetric surface dimer and a metal system of fcc Cu crystal of 1568 atoms.

### A. Asymmetric surface dimer on Si(001) surface

The molecular dynamics simulation with the shifted COCG method was tested in Si(001) surface reconstruction of a slab system of 1024 atoms with the transferable tight-binding Hamiltonian. [19] Atoms on the Si (001) surface form asymmetric dimers. [21, 22] Figure 3(a) shows the imaginary part of the Green's function ( $(1 - )\text{Im } G_{jj}$ ) corresponding to the local density of states (LDOS) of atoms forming the resultant asymmetric dimer on the (001) surface and, as for the positions and the heights, the result is in almost perfect agreement with the one obtained by the SD-KS method. [11] In the dimerized surface atoms,  $(1 - )\text{Im } G_{jj}$  of the upper (lower) atom has a peak just below (above) the Fermi energy, corresponding to an occupied (unoccupied) surface state. It should be noticed that the total number of peaks in  $(1 - )\text{Im } G_{jj}$  equal exactly the number of iteration steps or the dimension of the KS.

The necessary number of the iteration steps is different from states to states. When the number of the iteration steps or the dimension of the KS is larger than 30, the results show a reliable energy difference between two atoms of an asymmetric dimer. The resultant tilt angle of the asymmetric dimers is  $\approx 13.4^\circ$  and the reported experimental values are ranging from 5 to 19. [23] These

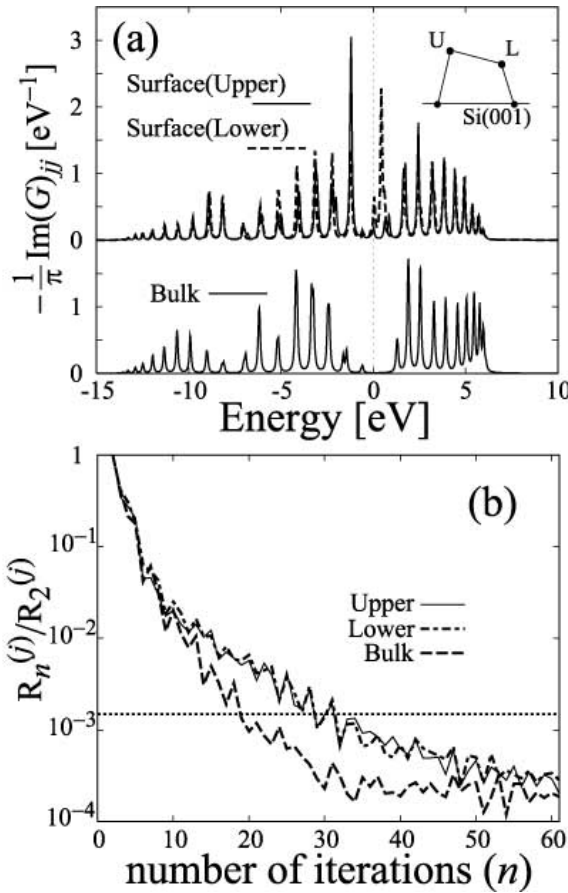


FIG . 3: (a) Imaginary part of the Green's function ( $\text{Im} G_{jj}$ ) (corresponding to the local density of states (DOS) per atom) for a slab system of 1024 Si atom with asymmetric dimer on (001) surface ( $\epsilon = 0.0544 \text{ eV}$ , the number of iteration steps  $n = 30$  and  $T = 1580 \text{ K}$  ( $\approx 0.136 \text{ eV}$ )). Solid line (broken line) in upper panel of (a) represents that of an upper (lower) atom of the asymmetric dimer. The peak shown at  $1.82 \text{ eV}$  ( $\approx 0.45 \text{ eV}$ ) in  $\text{Im} G_{jj}$  of upper (lower) atom corresponds to the occupied (unoccupied) surface state. The solid line in lower panel of (a) represents that of an atom on deeper layers of the present slab system (labeled as Bulk). (b) Dependence of a-RN on the number of iteration steps for the upper and the lower atoms of a dimer and an atom in a deeper layer of the slab. The horizontal dotted line is an eye guide to indicate the value of the a-RN  $R_n^{(j)} = R_2^{(j)} \cdot 10^{-3}$  for the surface dimer at  $n = 30$ .

DOS are different from that of the deeper layer of the slab system or that of the bulk crystal. Figure 3(b) shows the energy averaged RN (a-RN) during MD simulation, which presents the differences of the convergence behavior between surface dimer and bulk atoms. The a-RN for upper and lower atoms decays in a similar way, while that for the bulk part decays faster. Considering the fact that the required number of iterations is  $n = 30$  to obtain appropriate surface states such as the tilt angle and the surface energy, we can estimate that the optimal number of iterations is approximately 18 to obtain the same e

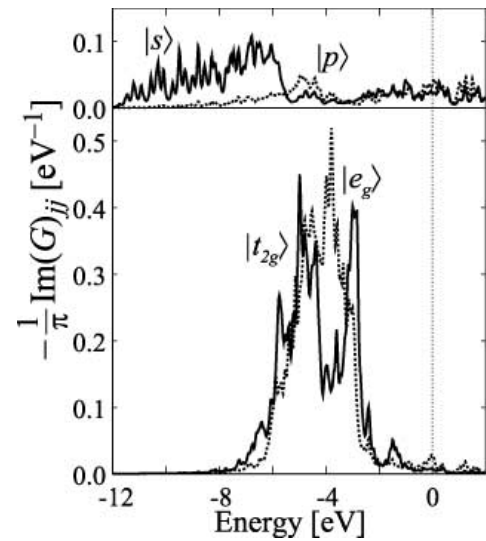


FIG . 4: Partial density of states  $\frac{1}{\pi} \text{Im} G_{jj}$  of 1568 atoms for fcc Cu.

accuracy of  $R_n^{(j)} = R_2^{(j)} \cdot 10^{-3}$  for the bulk part.

#### B . M etal system : fcc Cu

We calculated also the electronic structure of a metallic system, i.e. fcc Cu of 1568 atoms, by using the present shifted COCG method. We adopt the second-order Hamiltonian  $H^{(2)}$  of the tight-binding LMTO method. [20] The partial DOS is shown in Fig. 4 for s, p,  $e_g$  and  $t_{2g}$  orbitals. The essential characteristics, e.g. the resonance behavior of s and p orbitals and the energy separation between  $e_g$  and  $t_{2g}$  orbitals, can be reproduced.

Another important property for analysing cohesion is the crystal orbital Hamiltonian populations (COHP) defined as follows; [24]

$$C_{IJ}(\epsilon) = - \sum_{J \neq I} \text{Im} G_{I,J}(\epsilon) H_{J,I}; \quad (16)$$

$$C_{IJ}(\epsilon) = C_{IJ}(\epsilon); \quad (17)$$

where I and J denote the atomic positions and and orbitals. The energy integration of the COHP gives the cohesive energy, e.g. its negative/positive part corresponds to contributions of attractive/repulsive part for cohesion.

Figure 5(a) shows the COHP  $C_{IJ}(\epsilon)$  for the first nearest neighbor pair and the integrated COHP. Figure 5(b) shows the partial COHP's  $C_{IJ}(\epsilon)$  for the first nearest neighbor pairs. The inter-atom axis is along the (011) direction and, therefore, the cohesive mechanism works in  $s$ ,  $(p_y - p_z)/2$  and  $d_{yz}$  orbitals. The cohesion originates from d-electrons, mainly contributed by the  $t_{2g}$  orbitals directing to the first nearest neighbor. We can also observe the sharp positive peak in the COHP at

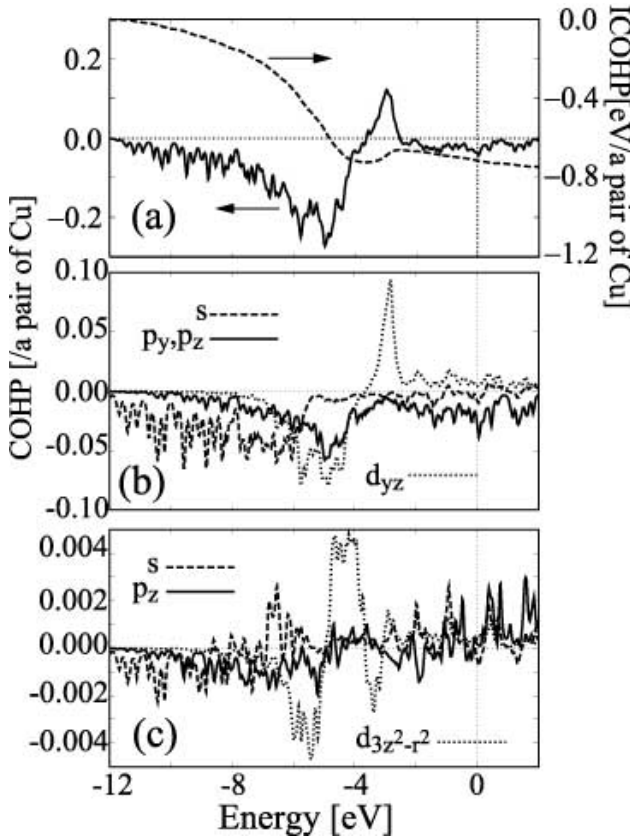


FIG. 5: The COHP and integrated COHP of 1568 atoms for fcc Cu (a). The partial COHP for the 1st (b) and the second neighbor atom pairs (c) are shown, respectively, for only parts of majority contribution. Note the difference of number of ordinate in (b) and (c).

Energy at 3 eV originates from the antibonding character of the  $t_{2g}$  orbitals directing to the 1st nearest neighbor. Contributions from s and p orbitals are also appreciable. Figure 5(c) shows the partial COHP's  $C_{IJ}$  (!) for the second nearest neighbor pairs whose inter-atom axis is along the (001) direction. Then the cohesive mechanism works in s,  $p_z$  and  $d_{3z^2-r^2}$  orbitals with magnitude one order smaller than those for the 1st neighbor pair. This kind of property can be easily calculated with the present shifted COCG method and so is true even for the force calculation in molecular dynamics simulation.

## V. CONCLUSIONS

In the present paper, we introduced the shifted COCG method based on the Krylov subspace into numerical calculation of the Green's function as a method with real-time error-control during molecular dynamics simulation. We proposed a procedure of accuracy evaluation by means of the a-RN and investigated its characteristics. The choice of the reference energy is arbitrary and the method is robust against the round-off error. We ap-

plied the method to a system of Si slab of 1024 atoms with asymmetric surface dimers. The dependence of the number of iteration steps on starting site was observed and the convergence was monitored by observing the difference between surface dimer and bulk part. We applied the method also to a fcc Cu system of 1568 atoms and examined the difference in convergence of each orbital symmetry. The convergence estimation was introduced also to the SD-KS method in Appendix B and analyzed the divergence behavior of the a-RN. If one would terminate the iteration step at the earlier stage, e.g. 30, the accuracy of the methods, the shifted COCG and the SD-KS methods, are the same. The difference would come appear when we go further stage of the iteration steps. Since they are general mathematical methods based on the linear algebra, these newly developed methods, the shifted COCG method and the SD-KS method, are applicable not only to molecular dynamics simulation with atomic orbitals but also to that with the numerical basis sets or even other systems of linear equations.

Although they are based on the Krylov subspace, both methods have their own advantage and disadvantage in practical calculation and two methods are complementary in actual MD simulation. For example, the shifted COCG is highly useful for focusing on targeting energy range because the choice of energy range is arbitrary. On the other hand, the SD-KS method is suitable for obtaining the whole spectral structure, though the method might suffer from round-off error as is discussed in Appendix B. In both methods, one can see the degree of the accuracy of calculation with a help of the a-RN.

## Acknowledgments

Computation was done at the Center for Promotion of Computational Science and Engineering (CCSE) of Japan Atomic Energy Research Institute (JAERI) and also partially carried out by use of the facility of the Supercomputer Center, Institute for Solid State Physics, University of Tokyo. This work is financially supported by Grant-in-Aid from the Ministry of Education, Culture, Sports, Science and Technology and also by ACT-JST and CREST-JST.

## APPENDIX A : FORMULATION OF THE SHIFTED COCG METHOD

### 1. Algorithm of the shifted COCG method

In this appendix we present the formulation of the shifted COCG algorithm, following Ref. [18]. The original paper [18] gives the formulation for a general non-Hermitian matrix A, which is called shifted BiCG algorithm. In the present context, however, the matrix A is complex symmetric and the formulation of the shifted COCG algorithm may be adopted.

For a given 'reference' linear system  $Ax = b$  we use the conventional COCG algorithm. Within the  $n$ -th iteration, the  $n$ -th solution vector  $x_n$ , the residual vector  $r_n$ , and the search direction vector  $p_n$  are represented as

$$x_n = x_{n-1} + r_{n-1} p_{n-1}; \quad (A 1)$$

$$r_n = r_{n-1} - A p_{n-1}; \quad (A 2)$$

$$p_n = r_n + r_{n-1} p_{n-1}; \quad (A 3)$$

respectively. Here, coefficients  $r_n$  and  $p_n$  are given as

$$r_n = \frac{r_n^T r_n}{p_n^T A p_n}; \quad (A 4)$$

$$p_n = \frac{r_{n-1}^T r_{n-1}}{r_n^T r_n}; \quad (A 5)$$

The initial conditions for iteration are  $x_0 = p_0 = 0$ ,  $r_0 = b$ ,  $r_1 = 0$ ,  $p_1 = 1$ . Note here that the vector products are given as  $a^T b \neq a^H b$ . Eliminating  $p_{n-1}$  from eq. (A 2) with (A 3), we obtain three-term recurrence relation for the residual vector;

$$r_{n+1} = r_n - \frac{1 + \frac{r_{n-1}^T r_n}{r_n^T r_{n-1}}}{1 + \frac{r_{n-1}^T r_n}{r_n^T r_{n-1}}} r_n - \frac{r_{n-1}^T r_n}{1 + \frac{r_{n-1}^T r_n}{r_n^T r_{n-1}}} r_{n-1}; \quad (A 6)$$

Similarly, for a given 'shifted' system  $(A + I)x = b$ , ( $A = A + I$ ), the  $n$ -th solution vector  $x_n$  and the search direction vector  $p_n$  are given as

$$x_n = x_{n-1} + r_{n-1} p_{n-1}; \quad (A 7)$$

$$p_n = r_n + r_{n-1} p_{n-1}; \quad (A 8)$$

The initial values of the vectors or coefficients are chosen as in the reference system. The equation corresponding to eq. (A 6) within the shifted system is

$$r_{n+1} = r_n - \frac{1 + \frac{r_{n-1}^T r_n}{r_n^T r_{n-1}}}{1 + \frac{r_{n-1}^T r_n}{r_n^T r_{n-1}}} r_n - \frac{r_{n-1}^T r_n}{1 + \frac{r_{n-1}^T r_n}{r_n^T r_{n-1}}} r_{n-1}; \quad (A 9)$$

Due to the equivalence of the KS between the reference and the shifted systems, one can prove that the residual vectors  $r_n$  and  $r_{n-1}$  are collinear; [18]

$$r_n = \frac{1}{n} r_{n-1}; \quad (A 10)$$

With eq. (A 10), eq. (A 6) can be modified as

$$\begin{aligned} r_{n+1} &= \frac{1}{n+1} (A + I) r_n \\ &+ \frac{1}{n+1} \left( 1 + \frac{r_{n-1}^T r_n}{r_n^T r_{n-1}} \right) r_n \\ &- \frac{r_{n-1}^T r_n}{n+1} \frac{r_{n-1}^T r_n}{n+1} r_{n-1}; \end{aligned} \quad (A 11)$$

Comparing the coefficients in eqs. (A 11) and (A 9), we obtain under the critical condition  $r_0 = p_1 = 1$ ,

$$r_n = \frac{n}{n+1} r_n; \quad (A 12)$$

$$p_n = \frac{n}{n+1} p_n; \quad (A 13)$$

$$r_{n+1} = 1 + \frac{n}{n+1} + \frac{n-1}{n+1} r_n - \frac{n-1}{n+1} r_{n-1}; \quad (A 14)$$

With the relations of eqs. (A 10), (A 12), (A 13), and (A 14), the inner product and the matrix-vector product in eqs. (A 4) and (A 5) are not calculated for the iterative update in the shifted system, eqs. (A 7) and (A 8). The resultant reduction in the computational cost is shown in Table I; the number of operations of the inner product and the matrix-vector product is drastically reduced as  $(3M N_{\text{ene}} + 3M)$  and  $(M M_{\text{int}} N_{\text{ene}} + M M_{\text{int}})$ , respectively.

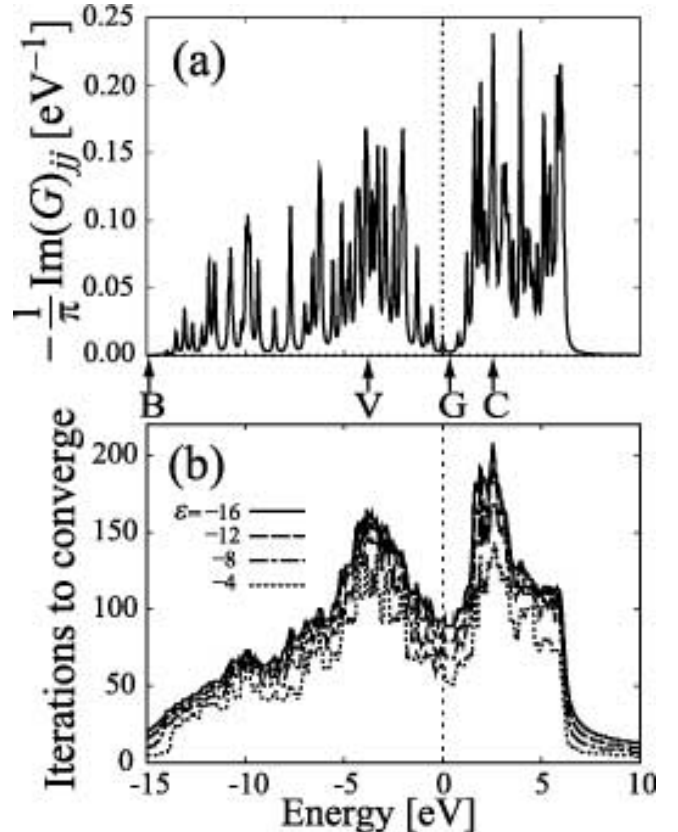


FIG. 6: A system of Si 512 atoms. (a)  $-\frac{1}{\pi} \text{Im } G_{jj}$  ( $\epsilon = 0.002\text{au}$ ). The top of the valence band locates at  $E = +0.4$  eV. (b) The number of iteration steps for the RN to converge with the criterion  $\frac{\|r_n^{(j)}\|}{\|r_n^{(0)}\|} < 10^{-6}$ .

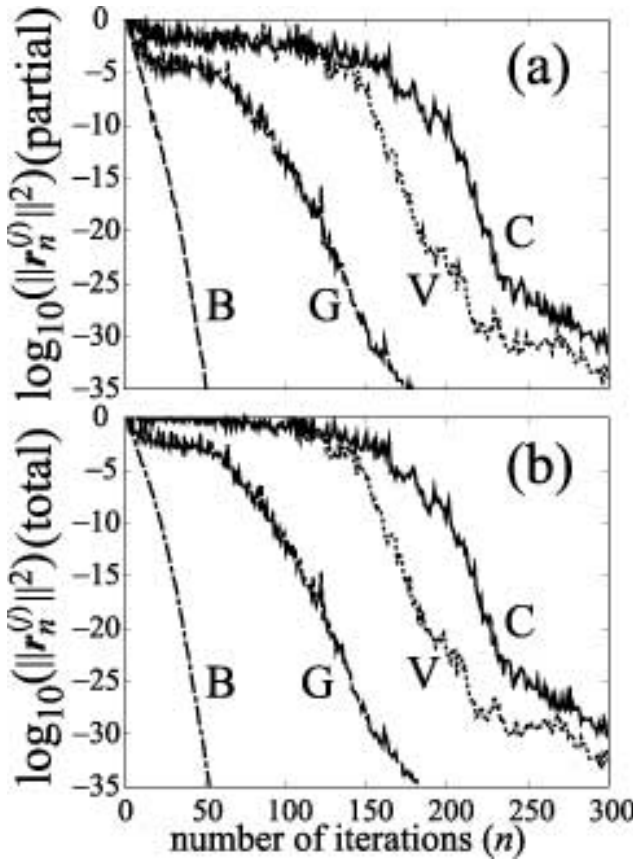


FIG. 7: Iteration dependence of (a) the residual norm RN and (b) the total residual norm t-RN for the selected reference energies shown by arrows in Fig. 6 (a).

## 2. Choice of convergence criterion

In Fig. 6 (a), we show the imaginary part of the Green's function, corresponding to the density of states. Since the  $N_{\text{ene}} = 1000$  energy points are selected with a small imaginary part  $\epsilon = 0.002$  au, the spectrum consists of a set of spikes. Though the four cases of the convergence criterion  $10^{-n}$  from  $10^{-4}$  to  $10^{-16}$  are applied in the CCG method, they are almost identical with each other. The iteration times for these several criteria are seen in Fig. 6 (b). An energy point with the larger density of states requires the more iteration times, i.e. the larger dimension of the KS, because the dimension of the KS should be larger in order to distinguish individuals among densely distributed nearby states.

Figure 7 (a) shows the comparison of decay behaviour of the RN for four chosen energy points B, V, G and C in the band region shown in Fig. 6 (a). The energy point of the larger DOS requires the larger iteration number or the larger KS as is shown in Fig. 6 (b) and the results are consistent. On the other hand, the energy point (B) makes the Green's function calculation converge very rapidly, reaching the limit of machine accuracy. However,

as shown in Fig. 1 the energy averaged residual norm a-RN is independent on the choice of the reference energy. In actual calculation, our choice of the number of iteration steps is a several tens and not more. The rapid decrease of the a-RN at the number of iterations  $< 10$  is the characteristic behavior and this is because that we care only the elements between near-sited orbital pairs connected directly by the short-ranged Hamiltonian.

Once we need the convergence for whole wavefunctions with the behavior of the tail, we should define the total residual norm (t-RN) for monitoring the convergence behavior instead of the RN eqs. (11) and (12):

$$\hat{r}_n^{(j)} \hat{r}_n^{(j)} = \sum_i \hat{r}_{n,i}^{(j)} \hat{r}_{n,i}^{(j)}; \quad (A15)$$

$$\hat{r}_n^{(j)} \hat{r}_n^{(j)} = \sum_i \hat{r}_{n,i}^{(j)} \hat{r}_{n,i}^{(j)}; \quad (A16)$$

where the upper limit of the summation is  $M$ , i.e. the size of the Hamiltonian. The comparison of decay behaviour of the total RN for the four chosen energy points is found in Fig. 7 (b). The decay behavior at the earlier stage is slower than that in Fig. 7 (a). However, the behavior at the later stage is the same. The accurate description of the behavior of wavefunctions at further distances needs the larger number of basis vectors and it takes the larger number of iterations. This is the reason why the convergence becomes slower at earlier iteration stage in Fig. 7 (b). However, we do not need all  $M$  components appearing in the residual vector to calculate physical properties because of the locality of the short-ranged tight-binding Hamiltonian. The number of operations in calculation of the t-RN is enormous, comparing with the 'present' method as shown in Table I.

## APPENDIX B : SUBSPACE DIAGONALIZATION METHOD AND CONVERGENCE ESTIMATION

### 1. Subspace diagonalization method

In the previous paper, we introduced the subspace diagonalization method (SD-KS method) on the basis of the Krylov subspace. [11] The procedure of generating the KS consumes the CPU time mostly when the Hamiltonian matrix is large. The orthonormalized basis set of the KS is generated with the three-term recurrence relation called the Lanczos process. This process creates simultaneously the reduced Hamiltonian matrix  $H^{(j)}$  in the KS. Then the eigenvalue  $\lambda^{(j)}$  and eigenvector  $jw^{(j)}$  are given by its diagonalization  $H^{(j)} jw^{(j)} i = \lambda^{(j)} jw^{(j)} i$ . The eigenvector  $jw^{(j)} i$  can be expanded in terms of the basis  $jK_n^{(j)} i$  of the KS;

$$jw^{(j)} i = \sum_{n=1}^X C_n jK_n^{(j)} i; \quad (B1)$$

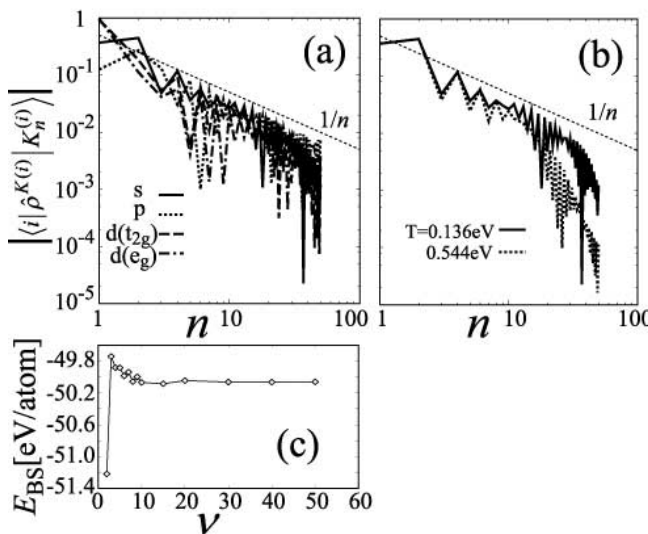


FIG. 8: (a) Decay properties of the off-diagonal density matrix,  $\langle i| \hat{\rho}^{K(j)} |K_n^{(j)} \rangle$ , of 8788 atom for fcc Cu as a function of  $n$  in the summation of eq.(B 4) representing number of hoppings from center atom. The initial orbital are  $j_{\text{si}}$  (solid line),  $j_{\text{pi}}$  (dotted line),  $j_{\text{d}}(t_{2g})_{\text{i}}$  (broken line), and  $j_{\text{d}}(e_g)_{\text{i}}$  (one dot chain line), respectively. (b) "Temperature" dependence of the decay property of  $\langle i| \hat{\rho}^{K(j)} |K_n^{(j)} \rangle$  for the  $s$ -orbital. (c) Matrix size,  $N$ , dependence of the calculated band structure energy.

We introduce the density matrix operator  $w$  within the KS:

$$\langle K^{(j)} | \sum_{j \in W^{(j)}} i \hbar w^{(j)} | j \rangle = \frac{w^{(j)}}{k_B T} : \quad (\text{B } 2)$$

The essence of the SD-KS method is the replacement of the density matrix  $h_{j,j}^{(j)}$  by that of the KS  $h_{j,j}^{(j)}$  as

$$h_{j,j}^{(j)} = h_{j,j}^{(K(j))} \quad (\text{B } 3)$$

$$= \sum_n h_{j,j}^{(K(j))} j K_n^{(j)} i \hbar K_n^{(j)} j i : \quad (\text{B } 4)$$

Once this procedure is allowed, it is great advantage from the view point of practical calculation. The Green's function within the SD-KS method is defined as

$$G^{(j)}(z) = \sum_n \frac{j w^{(j)} i \hbar w^{(j)} j}{z - w^{(j)}} : \quad (\text{B } 5)$$

The replacement eq. (B 3) is rigorous when  $w$  is equal to the dimension of the original Hilbert space. When  $w$  is much smaller, this replacement (B 3) can be justified only if the convergence of the summation in eq. (B 4) is fast enough and the contribution from large  $n$  is negligible. The decay property of the off-diagonal elements of the density matrix  $h_{j,j}^{(K(j))} j K_n^{(j)} i$  is shown for fcc Cu 8788 atom system in Fig. 8.

Although the decay behaviour of  $j_{jn}^{(K(j))} j = h_{j,j}^{(K(j))} K_n^{(j)} i j$  for different initial orbitals differs

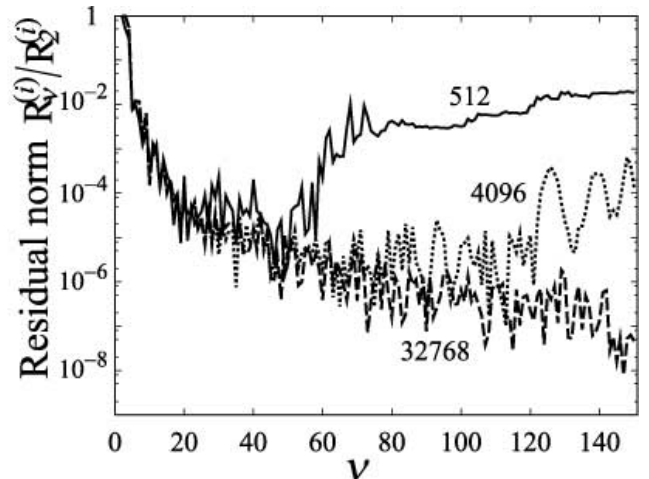


FIG. 9: Averaged residual norm a-RN by the subspace diagonalization method for Si crystals in different system sizes (atom number 512, 4096, 32768).

from each other in small  $N$  region, it decays generally as  $1=N$  in large  $N$  region (Fig. 8(a)). Note that, in semiconductors this decays as  $1=N^2$ . The element  $j K_n^{(j)} j i j$  here in a metal decays as  $1=N$  (not shown) and the products  $h_j j^{(K(j))} j K_n^{(j)} i \hbar K_n^{(j)} j i j$  in eq.(B 4) decays as  $1=N^2$ . When we use higher "temperatures" in the Fermi distribution function, the decaying behavior becomes much faster as in semiconductor as shown in Fig. 8(b). [11] These facts validate the convergence of the summation in eq.(B 4) and justifies the replacement eq.(B 3). Therefore, the calculated properties converge to finite value as a function of reduced matrix size. See, for example, dependence of the calculated band structure energy shown in Fig. 8 (c).

## 2. Convergence estimation in the subspace diagonalization method

The RN in the SD-KS method can be defined from eqs. (B 1) and (B 5) as

$$\begin{aligned} h_{j,j}^{(j)} i &= h_{j,j}^{(j)} (z - H) G^{(j)}(z) j i \\ &= h_{j,j}^{(j)} i \sum_{n=1}^N \frac{h_{j,j}^{(j)} H K_n^{(j)} i}{z - w^{(j)}} \sum_{m=1}^M h K_m^{(j)} j i : \end{aligned} \quad (\text{B } 6)$$

The term  $H K_n^{(j)} i$  appearing in the numerator can be evaluated simultaneously in the updating process of  $K_n^{(j)} i$ . The a-RN  $R^{(j)}$  in the SD-KS can be defined as similar way as eq. (13) by using  $h_{j,j}^{(j)} i$ . We examined several cases in different system size as shown in Fig.9 (512, 4096, and 32768 atoms). There should be an optimal value of the dimension of the KS. Once the dimension of the KS exceeds an appropriate value, the residual norm

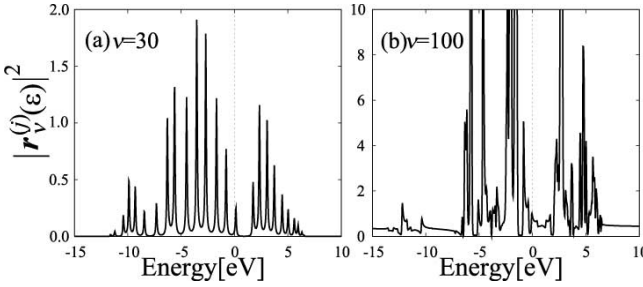


FIG. 10: Energy dependence of the residual norm of Sicrystal of 512 atom with subspace diagonalization. The size of subspace are (a)  $\nu = 30$  and (b)  $\nu = 100$ . Note the different scale in the ordinates.

grows again. The starting point of growing the error and its growing rate depend on the system size as seen in Fig. 9. In other words, the SD-KS method shows rapid convergence behavior but, if one needs to know very details of the spectrum by using a large KS, it may cause another trouble. The behavior is attributed to the loss of orthogonality among the basis vectors generated by the Lanczos process (three-term recurrence relation) due to a gradual accumulation of round-off error.

The RN are shown in Fig. 10, where in (a) the spectrum consists of only spikes while in (b) of a finite background as well as spikes. This constant background is due to the loss of orthogonality among the basis vectors generated by the Lanczos process, and the loss of orthogonality is attributed to the result of the gradual accumulation of round-off error.

In order to show the origin of the finite background appearing in  $\mathbf{j}_{\nu}^{(j)}$ , we start with introducing the deviation  $\mathbf{j}_{\nu}^{(j)}$  from true wave function. The eigenvalue equation with a round-off error  $\mathbf{j}_{\nu}^{(j)}$  can be rewritten as

$$\mathbf{H}^{(j)} \mathbf{j}_{\nu}^{(j)} = \mathbf{H} \mathbf{j}_{\nu}^{(j)} + \mathbf{j}_{\nu}^{(j)} \quad (B7)$$

Using eqs. (B5), (B6) and (B7), the residual norm for the SD-KS can be rewritten as

$$\begin{aligned} \mathbf{h}_{\nu}^{(j)} \mathbf{j}_{\nu}^{(j)} &= \mathbf{h}_{\nu}^{(j)} (\mathbf{z} - \mathbf{H}) \mathbf{G}^{(j)} (\mathbf{z}) \mathbf{j}_{\nu}^{(j)} \\ &= \mathbf{h}_{\nu}^{(j)} \mathbf{j}_{\nu}^{(j)} \sum_{i=1}^X \mathbf{h}_{\nu}^{(j)} \mathbf{i} \mathbf{h}_{\nu}^{(j)} \mathbf{i} \mathbf{j}_{\nu}^{(j)} + \sum_{i=1}^X \frac{\mathbf{h}_{\nu}^{(j)} \mathbf{i} \mathbf{h}_{\nu}^{(j)} \mathbf{i} \mathbf{j}_{\nu}^{(j)}}{\mathbf{z} - \mathbf{H}^{(j)}} \\ &= \mathbf{h}_{\nu}^{(j)} \mathbf{j}_{\nu}^{(j)} + \sum_{i=1}^X \frac{\mathbf{h}_{\nu}^{(j)} \mathbf{i} \mathbf{h}_{\nu}^{(j)} \mathbf{i} \mathbf{j}_{\nu}^{(j)}}{\mathbf{z} - \mathbf{H}^{(j)}}, \end{aligned} \quad (B8)$$

where, since  $\mathbf{K}_1^{(j)} \mathbf{i} = \mathbf{j}_{\nu}^{(j)}$ ,

$$\mathbf{j}_{\nu}^{(j)} = \mathbf{j}_{\nu}^{(j)} \sum_{i=1}^X \mathbf{j}_{\nu}^{(j)} \mathbf{i} \mathbf{h}_{\nu}^{(j)} \mathbf{i} \mathbf{j}_{\nu}^{(j)} = \sum_{i=1}^X \mathbf{K}_n^{(j)} \mathbf{i} \mathbf{h}_{\nu}^{(j)} \mathbf{i} \mathbf{j}_{\nu}^{(j)} \quad (B9)$$

The vector  $\mathbf{j}_{\nu}^{(j)}$  should vanish when all elements of the KS  $\mathbf{K}_n^{(j)} \mathbf{i}$  is orthogonal to the first one  $\mathbf{K}_1^{(j)} \mathbf{i} = \mathbf{j}_{\nu}^{(j)}$  and the spectrum consists of spikes only, i.e. the second term of eq. (B8). However, the loss of orthogonality always happen in actual calculation after a long iterative procedure. After all, an energy independent contribution  $\mathbf{h}_{\nu}^{(j)} \mathbf{j}_{\nu}^{(j)}$  can be seen in Fig. 10 (b).

---

[1] W. Kohn, Phys. Rev. Lett. 76, 3168 (1996).  
 [2] R. Haydock, Solid State Phys. 35, 129 (1980).  
 [3] G. Galli, Phys. Status Solidi B 217, 231 (2000).  
 [4] S. Y. Wu and C. S. Jayamani, Phys. Rep. 358, 1 (2002).  
 [5] O. K. Andersen, T. Saha-Dasgupta, R. W. Tank, C. Arcangeli, O. Jepsen and G. Krier: in Electronic Structure and Physical Properties of Solids, eds. H. Dresse (Springer-Verlag, 2000) pp 3-84.  
 [6] T. Hoshi and T. Fujiiwara, J. Phys. Soc. Jpn. 69, 3773 (2000).  
 [7] T. Hoshi and T. Fujiiwara, Surf. Sci. 493, 659 (2001).  
 [8] T. Hoshi and T. Fujiiwara, J. Phys. Soc. Jpn. 72, 2429 (2003).  
 [9] T. Hoshi, Theory and application of large-scale electronic structure calculation, Doctor thesis, University of Tokyo, 2003.  
 [10] M. Geshi, T. Hoshi, and T. Fujiiwara, J. Phys. Soc. Jpn. 72, 2880 (2003).  
 [11] R. Takayama, T. Hoshi, and T. Fujiiwara, J. Phys. Soc. Jpn. 73, 1519 (2004).  
 [12] D. Mayou, Europhys. Lett. 6, 549 (1988).  
 [13] S. Roche and D. Mayou, Phys. Rev. Lett. 79, 2518 (1997).  
 [14] H. A. van der Vorst, Iterative Krylov Methods for Large Linear Systems, Cambridge University Press, Cambridge, 2003.  
 [15] H. A. van der Vorst and J. B. M. Elissen, IEEE Transactions on Magnetics, 26, 706 (1990).  
 [16] Y. Saad: Iterative Methods for Sparse Linear Systems (second edition), SIAM, Philadelphia, 2003.  
 [17] R. W. Freund, in Numerical Linear Algebra, L. Reichel, A. Rutman, and R. S. Varga eds. de Gruyter, Berlin, pp. 101-121 (1993).  
 [18] A. Frommer, Computing 70, 87 (2003);  
<http://www.math.uni-wuppertal.de/SciComp/>.  
 [19] I. Kwon, R. Biswas, C. Z. Wang, K. M. Ho, and C. M. Soukoulis, Phys. Rev. B 49, 7242 (1994).  
 [20] O. K. Andersen and O. Jepsen, Phys. Rev. Lett. 53, 2571 (1984).  
 [21] D. J. Chadi, Phys. Rev. Lett. 43, 43 (1979).  
 [22] A. Ramm, G. Brocks and P. J. Kelly, Phys. Rev. B 51, 14504 (1995).  
 [23] J. Polman, P. Kugler, M. Rohling, M. Sabisch, and D. Vogel, Appl. Surf. Sci. 104-105, 1 (1996).  
 [24] R. Dronskowski and P. E. Blöchl, J. Phys. Chem. 97, 8617 (1993).